Mechanism of Magnetic Relaxation Switching Sensing

Changwook Min,[†] Huilin Shao,[†] Monty Liong,[†] Tae-Jong Yoon,[†,§] Ralph Weissleder,[†,‡,*] and Hakho Lee[†,*]

[†]Center for Systems Biology, Massachusetts General Hospital, 185 Cambridge Street, Boston, Massachusetts 02114, United States and [‡]Department of Systems Biology, Harvard Medical School, Boston, Massachusetts 02115, United States. [§]Present address: Department of Applied Bioscience, CHA University, Seoul 135-081, Republic of Korea.

ABSTRACT

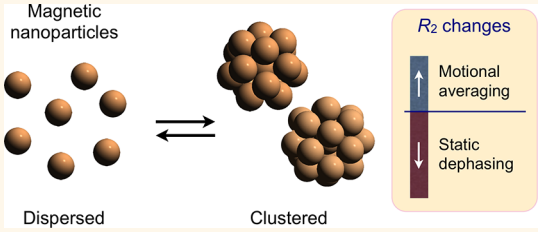

Magnetic relaxation switching (MRSw) assays that employ target-induced aggregation (or disaggregation) of magnetic nanoparticles (MNPs) can be used to detect a wide range of biomolecules. The precise working mechanisms, however, remain poorly understood, often leading to confounding interpretation. We herein present a systematic and comprehensive characterization of MRSw sensing. By using different types of MNPs with varying physical properties, we analyzed the nature and transverse relaxation modes for MRSw detection. The study found that clustered MNPs are universally in a diffusion-limited fractal state (dimension of ~2.4). Importantly, a new model for transverse relaxation was constructed that accurately recapitulates observed MRSw phenomena and predicts the MRSw detection sensitivities and dynamic ranges.

KEYWORDS: magnetic relaxation switching · magnetic nanoparticles · NMR · biosensors

The advance of nanoparticles has significantly accelerated the development of new, highly sensitive biosensors that have broad applications in basic biomedical research, drug discovery, and clinical diagnostics.[1−3] With their size scale often similar to those of biological molecules, nanoparticles can efficiently bind to target biomarkers, generating distinctive and amplified analytical signals.[4] Magnetic nanoparticles (MNPs) in particular offer an attractive sensing mechanism.[5,6] Owing to the intrinsically low magnetic susceptibility of biological media, MNPs can achieve high "contrast" even in complex biological specimens with little interference from biological background.

We have previously developed a MNP-based sensing methodology for water-soluble biomarkers.[7,8] The approach is based on the phenomenon of magnetic relaxation switching (MRSw) as a sensing mechanism; when MNPs cross-link upon the recognition and binding of biological targets, these clustered particles change the transverse (R_2) relaxation of water protons, which can be detected by nuclear magnetic resonance (NMR; Scheme 1). Alternatively, the assay can be performed in reverse mode, where enzymatic cleavage or competitive binding of molecular targets disassembles preformed clusters. The assay is ideally suited for detecting small biological targets; the formation of MNP clusters is most efficient when size of the detection targets is smaller than that of MNPs, and the assay does not require extensive purification to separate the bound from the free MNPs. Moreover, since the signal is generated from the entire sample volume, the assay benefits from faster binding kinetics than that of surface-structure-based devices. Many different types of targets, including small molecules, nucleic acids, and proteins, have thus been detected by MRSw.[7,9−12]

To date, however, the precise working mechanisms of MRSw have not been fully characterized. This results in a limited understanding of MRSw detection capacities, which is further confounded by conflicting literature reports on R_2 changes upon MNP clustering.[12−14] Specifically, most prior reports were limited by studying only one type of MNPs (*e.g.*, with a fixed core size) or a single transverse relaxation mode (*i.e.*, motional averaging) regardless of the MNP cluster size.[13−15]

We herein report on a systematic and comprehensive characterization of the MRSw assay. A panel of MNPs with different physical properties were synthesized and utilized for comparative analyses. We specifically focused on (1) characterizing the

* Address correspondence to hlee@mgh.harvard.edu, rweissleder@mgh.harvard.edu.

Received for review April 12, 2012 and accepted July 3, 2012.

Published online July 04, 2012
10.1021/nn301615b

© 2012 American Chemical Society

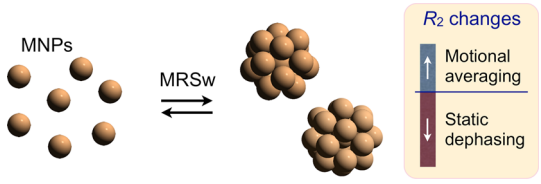

Scheme 1. Magnetic relaxation switching (MRSw) assay. Dispersed magnetic nanoparticles (MNPs; left) form clusters upon binding with target molecules (right). Depending on the cluster size, the transverse relaxation of samples can assume two separate modes, motional averaging and static dephasing, resulting in opposite changes in its relaxation rate (R_2).

nature of MNP clustering; (2) elucidating the different transverse relaxation modes with such clustered MNPs; and (3) establishing the relationship between a MNP's material properties and its MRSw detection sensitivities. Our study found that clustered MNPs are universally in a quasi-solid, fractal state (dimension of ~2.4). Accordingly, a new model for transverse relaxation was constructed that describes the observed MRSw phenomena. Most importantly, the study led to an analytical MRSw model that could predict the detection sensitivities and dynamic ranges for a given type of MNPs. These findings will aid in not only interpreting existing experiment data but also designing new MNPs and assay protocols to further improve MRSw sensitivities.

RESULTS

Preparation of MNPs with Different Relaxation Properties. We first synthesized a panel of MNPs with different size and composition (Figure 1a; see Methods for details). Small MNPs (CLIO; cross-linked iron oxide) were synthesized through chemical co-precipitation of ferric (Fe^{3+}) and ferrous (Fe^{2+}) chloride with the addition of a base solution (NaOH).[16] The magnetic core measured ~8 nm in diameter and was covered with a thick layer of 10 kDa dextran, crossed-linked with epicholorohydrin. The resulting particles had a hydrodynamic diameter of ~35 nm. Additional ferrite MNPs (Fe_3O_4) were synthesized *via* thermal decomposition of metal complexes (iron(III) acetylacetonate [$Fe(acac)_3$]) at high temperature (300 °C). The core size of these particles was increased from 12 to 16 and then 22 nm, through a seed-mediated growth approach.[17] In a similar manner, Mn-doped ferrite ($MnFe_2O_4$) particles, which have higher magnetization than Fe_3O_4, were also prepared by thermally decomposing $Fe(acac)_3$ in the presence of manganese complexes ($Mn(acac)_2$).[18] To further improve the magnetization, elemental iron (Fe) was selected as a core material of new nanoparticles. Initially, Fe-MNPs were synthesized by thermally decomposing iron(0) pentacarbonyl [$Fe(CO)_5$]. To prevent oxidation, Fe-MNPs were then encased with an artificially grown ferrite shell ($Fe@MnFe_2O_4$).[19] All prepared MNPs were rendered water-soluble by coating the particle

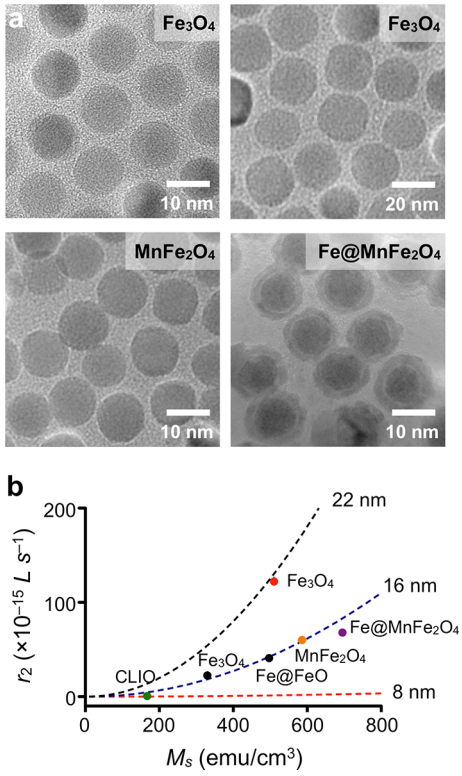

Figure 1. Panel of MNPs with different transverse relaxivities. (a) To study the effect of particle relaxivity (r_2) on MRSw assays, different types of MNPs with varying size and magnetization were synthesized. The transmission electron micrographs confirmed the narrow size distribution of the prepared MNPs. Clockwise from the top left are 16 nm Fe_3O_4, 22 nm Fe_3O_4, 16 nm Fe-core and $MnFe_2O_4$ shell ($Fe@MnFe_2O_4$), 16 nm $MnFe_3O_4$ MNPs. (b) The measured transverse relaxivity (r_2) showed good agreement with those predicted by an outer-sphere model (dashed lines). These MNPs thus were in the motional averaging regime in their nonclustered state. M_s, saturation magnetization; CLIO, cross-linked iron oxide nanoparticle.

surface with small molecules (2,3-dimercaptosuccinic acid) with the exception of CLIO, which had a hydrophilic dextran coating.

For each type of MNP, we measured its transverse relaxivity (r_2), the capacity of the particles to accelerate the R_2 relaxation of water protons (Methods). With different diameter (d_s; 8−22 nm) and magnetization (M), the prepared MNPs assumed a wide range of r_2 values (Figure 1b). All MNPs, however, were in the motional averaging regime of R_2 relaxation, where the diffusional motion of water protons was fast enough to average out the effects of MNPs. Consequently, the observed r_2 values could be fitted to $r_2 \approx d_s^2 M^2$, as predicted by the outer-sphere model (dotted lines, Figure 1b).[20]

Characterization of MNP Clusters and Relaxation Mechanism. Prepared particles were used to characterize the effect of different MNP types on the MRSw assay. As a model mechanism for particle clustering, we used the avidin−biotin interaction. MNPs were biotinylated by forming amide bonds between carboxylic acids in MNPs and

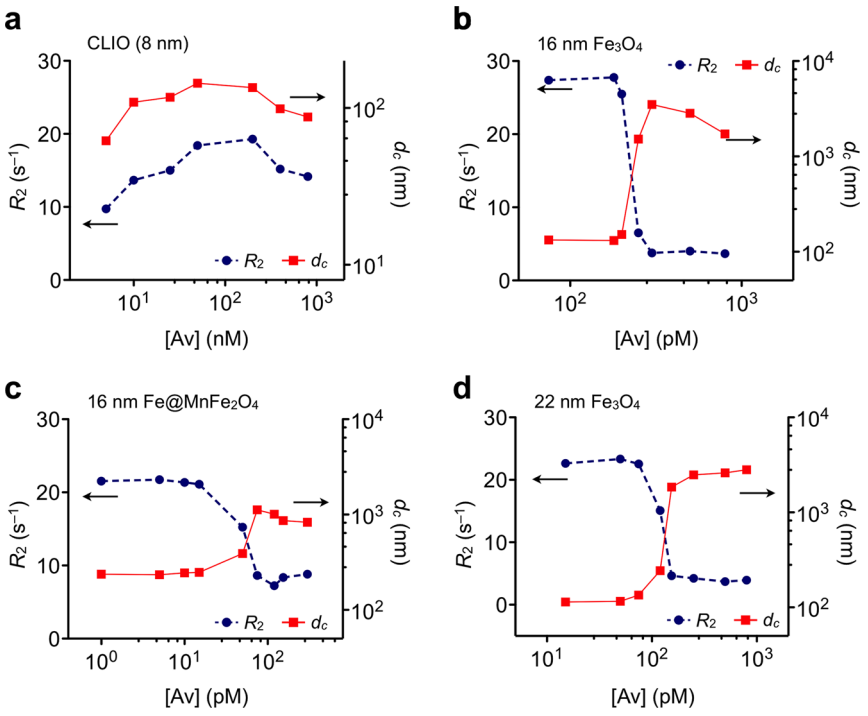

Figure 2. Different MRSw behaviors for a panel of MNPs. Two distinct relationships between R_2 and cluster size (d_c) were observed. With small MNPs (*e.g.*, 8 nm core MNP; CLIO), the R_2 values were commensurate with the cluster size (a), which indicated that the clusters remained in the motional averaging (MA) regime. For all other MNP types, R_2 values decreased with the cluster size (b−d) as the clusters entered a different relaxation mode (static dephasing; SD).

amine groups in biotin (Methods). On average, 40 biotin molecules were found to be immobilized per particle. For the MRSw assay, a varying amount of avidin was introduced to the biotinylated-MNP solution; control samples were prepared in the same way, but with the addition of a PBS (phosphate-buffered saline) solution (Methods). Following a 15 min incubation at $T = 300$ K, the samples were subjected to R_2 measurements using a miniaturized NMR system previously reported.[7,21] The corresponding size of MNP clusters was measured *via* dynamic light scattering (DLS).

Two distinct MRSw modes were observed (Figure 2). With small particles (CLIO), the R_2 values initially rose and then decreased with increasing avidin concentration ([Av]; Figure 2a). In contrast, larger MNPs showed an initial decrease and plateau of R_2 values with increasing [Av] (Figure 2b−d). For all types of MNPs, a strong correlation between R_2 and cluster size (d_c) was observed, which led to the development of a new physical model of MRSw phenomena. (1) For small MNPs, the clustered particles remain in the motional averaging (MA) mode of relaxation; these clusters are still small enough that the effect of their magnetic fields is averaged out by the diffusional motion of water molecules.[22] In the MA mode, the R_2 values concomitantly increase with the particle size. With a core size of 8 nm and water-permeable coating, the clustered CLIO falls into this regime, showing a close match between R_2 and d_c. Further addition of avidin, however, leads to a decrease of both R_2 and d_c, as excess avidin coats the MNPs (prozone effect) to hinder interparticle clustering.[23] (2) Larger MNPs assume a different relaxation mode upon clustering, namely, static dephasing (SD), as their cluster size exceeds the traveling distance of diffusing water molecules. These clusters appear as randomly distributed, stationary objects.[24] In the conventional SD model, where MNPs are assumed to be a solid sphere with a constant magnetization (M), the R_2 values are independent of the particle size but only proportional to M. For the MRSw, however, the observed R_2 values declined with the cluster size d_c, indicating that the effective M decreased in the corresponding clusters.

The observed new R_2-dependence on the cluster size was further analyzed in the framework of the diffusion-limited aggregation model.[25−27] Clusters of nanoparticles are known to have a fractal structure; the number of particles (n) per cluster is given as $n \approx (d_c)^f$, where f is the fractal dimension. Accordingly, we hypothesize that the magnetization M_c of the MNP clusters scales as $M_c = M_s(d_c/d_s)^{f-3}$, where M_s and d_s are the magnetization and the diameter of a single MNP, respectively (see Supporting Information for details). By denoting R_{2c} and R_{2s} as the relaxation rates for clusters and individual MNPs, respectively, we then obtain the following power law for the normalized relaxation rate and particle size. For the MA mode, R_2 is proportional to d^2M^2; hence $(R_{2c}/R_{2s})_{MA} \approx (d_cM_c)^2/(d_sM_s)^2 \approx (d_c/d_s)^{2f-4}$ (Figure 3a). Likewise $(R_{2c}/R_{2s})_{SD} \approx (d_c/d_s)^{f-3}$ for the SD mode, since R_2 is proportional to M (Figure 3b). When the observed MRSw data

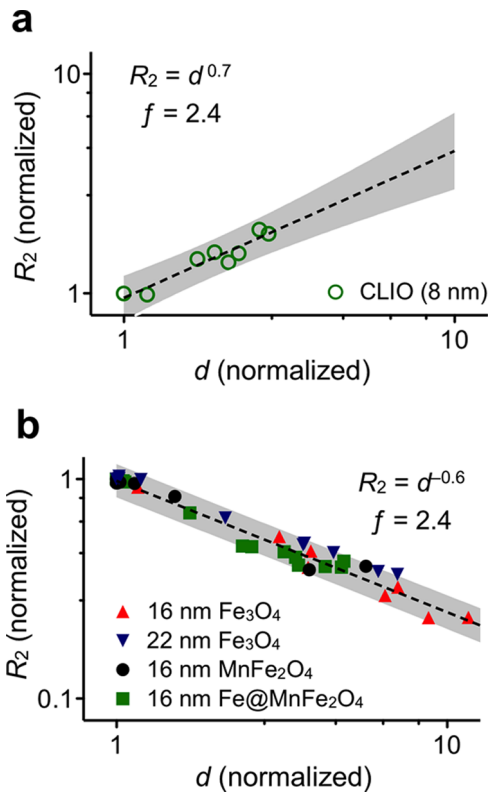

Figure 3. Characterization of MNP clustering. The normalized R_2 and d showed different power law behaviors than that expected from a conventional MA or SD model, which could be attributed to the fractal nature of MNP clusters. From the observed data, the dimension constant (f) was obtained. Clusters, both in MA (a) and SD (b) mode of relaxation, assumed a universal f value (= 2.4), which is close to the theoretical maximum (2.7). Gray areas indicate 95% prediction levels from the fit.

were replotted in these normalized units, it indeed showed the power law behavior. The dimension (f) determined for each MNP type had a universal value ($f \approx 2.4$), revealing the generic fractal nature of MNP clusters. Similar results were also observed when MRSw assays were performed using DNA molecules as a cross-linker (Figure S1). Clusters of small MNPs (8 nm Fe_3O_4) were found to be in the MA mode, whereas larger MNPs (16 nm $MnFe_2O_4$) fell into the SD mode upon clustering; the fractal dimension of MNP clusters for both modes was around 2.4. This value is in good agreement with those (f = 2.1−2.5) measured by other methods for nanoscale clusters.[27−29]

Analytical Model for MRSw Assays: Detection Sensitivities and Dynamic Ranges. To evaluate the utility of MRSw for molecular sensing, we next investigated the detection limit and dynamic range for each MNP type. For a given MNP concentration, an avidin-dose−response curve was obtained (Figure 4a, b). The lower and upper bounds of [Av] for detection were defined from 5% to 95% of the overall R_2 responses. The detection limit was found to improve with decreasing MNP concentrations, presumably due to a favorable stoichiometric ratio between MNPs and avidin molecules; the R_2 changes are maximized since all MNPs could be transformed into clusters under these conditions. Lowering MNP concentrations, on the other hand, reduced the dynamic ranges, as the R_2 of MNP solutions became closer to that of the background (*e.g.*, water). These opposing behaviors led to the following consequences: (1) MNPs with higher r_2 achieve lower detection limit by producing larger R_2 changes even at low particle concentrations; (2) each MNP type has an absolute lower detection limit, set by the diminishing dynamic ranges. The experimental data further confirmed this hypothesis. The detection limit scaled inversely with particle r_2; the lowest detection limit was ~1 pM with 22 nm Fe_3O_4 ($r_2 = 1.2 \times 10^{-15}$ L·s^{-1}), whereas 8 nm ferrite ($r_2 = 7.0 \times 10^{-16}$ L·s^{-1}) had the limit of ~2 nM.

The observed detection limits and dynamic ranges were further formulated into a general analytical model, based on the developed MRSw modes (MA, SD) for different MNPs (see Supporting Information for details). The model correlated well with experimental observation (Figure 4c); the detection limit was found to scale as $1/r_2$, and the dynamic range was proportional to k/α, where k and α are the average numbers of individual MNPs and avidin molecules per cluster, respectively. For the case of DNA molecules, their lower binding affinity led to the formation of smaller MNPs clusters, resulting in smaller k. The overall detection sensitivity and dynamic ranges were thus reduced.

The developed model can further estimate effective MRSw responses for a given MNP type and concentration (Figure 4c), which can facilitate assay determination and optimization for intended detection targets. Importantly, we could accurately predict the MRSw mode and the absolute detection limit as a function of particle relaxivity, r_2 (Figure 4d). The transition from MA to SD for MNP clusters happened at $r_2 \approx 10^{-15}$ L·s^{-1} (Supporting Information), and higher r_2 lowered the absolute detection limit, all of which agreed well with experimental data.

DISCUSSION

We have performed a systematic investigation on MRSw phenomena using a panel of MNPs with different size and magnetization (Table 1). The study showed that the cluster size of MNPs governs the transverse relaxation mode, namely, motional averaging and static dephasing, and thereby elucidated and unified contradicting R_2 changes in previous reports. The study also identified the universal fractal nature (f = 2.4) of MNP clusters, which led to a new formulation for MA and SD relaxation modes. On the basis of this understanding, we developed an analytical MRSw model that can be used to estimate the detection limit and dynamic range for a given MNP type. The model further indicates that the detection sensitivity can be enhanced by (1) using MNPs with high r_2 relaxivity, (2) optimizing the stoichiometric ratio

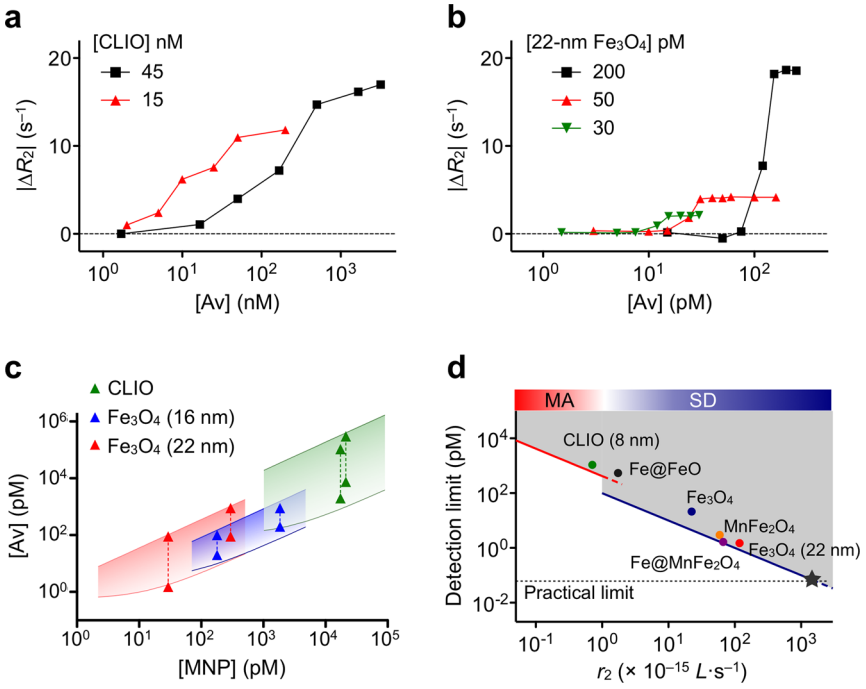

Figure 4. Analytical modeling of MRSw assays. (a, b) The detection threshold and dynamic range of each MNP type were determined. For both MA and SD modes, the detection sensitivity improved with decreasing MNP concentrations. With lower MNP numbers, however, the detection dynamic range became narrower with the R_2 of the MNP solution approaching that of background. These effects set the detection limit for each MNP type. (c) An analytical MRSw model (for MA and SD modes) was constructed that can estimate the detection limit and the dynamic range for a given MNP type and concentration. The model showed good correlation with the observed data (dotted lines with triangles). (d) The r_2 relaxivity of MNPs determines the relaxation mode of clusters, with the transition from MA to SD occurring around $r_2 \approx 10^{-15}$ L·s^{-1}. The MRSw model also revealed that the detection limit is proportional to $1/r_2$ (solid lines), which agreed well with the experiment data (filled circles). Notably, the sensitivity enhancement becomes progressively slower with r_2 increases, which places practical limits on further sensitivity improvement. The practical detection limit (~100 fM) was calculated assuming the use of hypothetical, highly magnetic Fe-MNPs (d_s = 22 nm). Nevertheless, these limits could be overcome by designing new assays employing target amplification strategies and magnetic microspheres.

TABLE 1. Physical Properties of Magnetic Nanoparticles and the Summary of MRSw Assays

magnetic nanoparticles				MRSw assay	
composition	core size (nm)	hydrodynamic diameter (nm)	r_2 relaxivity (× 10^{-15} s^{-1}·L)	assay mode[a]	detection limit (pM)[b]
Fe_2O_3/Fe_3O_4	8	35	0.7	MA	2000
Fe_3O_4	16	19	23	SD	20
$MnFe_2O_4$	16	19	60	SD	2.6
Fe_3O_4	22	25	123	SD	1.0
Fe@FeO	16	19	1.8	transition from MA to SD	500
$Fe@MnFe_2O_4$	16	19	68	SD	1.5

[a] MA, motional averaging; SD, static dephasing. [b] Based on avidin detection using biotinylated magnetic nanoparticles.

between MNPs and molecular targets, and (3) forming denser and larger MNP clusters, which could be achieved by maximizing binding sites per MNP.[30] Indeed, among the panel of tested nanoparticles, MNPs with the highest r_2 (22 nm Fe_3O_4) achieved the lowest detection limit (~1 pM, avidin); by lowering MNP concentration and thereby reducing the particle-to-target ratio, the detection sensitivities were also improved.

The model conversely reveals a practical limitation in sensitivity improvement. First, with the detection limit scaling as $1/r_2$, the benefit of increasing r_2 can be easily offset by technical difficulties in MNP synthesis. Preparing single MNPs with higher r_2 is a difficult task, which is often challenged by the availability of suitable magnetic materials and the colloidal stability of resulting particles. Second, because the detection limit is weakly dependent on f, only limited improvement in sensitivity can be achieved through densely packing MNPs. For instance, maximally packed clusters (f = 2.7) could be formed by switching from monodisperse to polydisperse particles.[31] The overall sensitivity improvement, however,

is expected to be less than 2-fold. Third, due to the intrinsic R_2 of the background (*e.g.*, 0.5 s^{-1} for water), there exists a lower bound on MNP concentration to generate discernible R_2 changes (*e.g.*, 5% above the background), which will in turn set the minimum amount of molecular targets detectable. Together, these factors place a practical detection limit in empirical MRSw assays (~100 fM) with MNPs (see Supporting Information for details).

CONCLUSIONS

To further improve MRSw sensitivity, we thus propose the following approaches. First, the assay could incorporate additional target-based amplification strategies. For instance, by employing DNA tags for molecular targeting and performing polymerase chain reaction for their amplification, both the detection sensitivity and specificity of the sensing platform could be considerably enhanced.[32] Second, magnetic microspheres, which are developed for magnetic separation, could be adapted for MRSw.[11,33,34] By embedding a large number of small magnetic cores, these particles assume larger r_2 relaxivities than MNPs and can offer higher detection sensitivity. However, judicious screening and optimization of particles should precede, as magnetic microspheres could display R_2 drift due to magnetic aggregation during relaxation measurements.[19] Combined with the advantages of MRSw (*i.e.*, negligible interference from biological background, no need for washing steps, and fast assay kinetics), these improved platforms would be a powerful analytic tool for molecular detection.

METHODS

Synthesis and Characterization of Magnetic Nanoparticles. All MNPs were prepared as previously reported. Briefly, amine-terminated cross-linked iron oxide nanoparticles were generated by aqueous co-precipitation and coated with dextran.[35]

Ferrite nanoparticles (Fe_3O_4 and $MnFe_2O_4$) were synthesized *via* thermal decomposition and enlarged through a seed-mediated growth process.[18] Iron(III) acetylacetonate [99.9%, Fe(acac)3], manganese(II) acetylacetonate [Mn(acac)3], oleylamine (70%), 1-octadecene (95%, ODE), 1,2- hexadecanediol (90%), chloroform (99%), sulfosuccinimidyl-(4-*N*-maleimidomethyl)-cyclohexane-1-carboxylate (99%, sulfo-SMCC), 2,3-dimercaptosuccinic acid (98%, DMSA) and dimethyl sulfoxide (99.9%, DMSO) were purchased (Sigma–Aldrich) and used without further modification. 2-Propanol (99.5%), hexane (98.5%), ethanol (99.5%), and $NaHCO_3$ were purchased (Fisher Scientific) and used as received.

We first synthesized 10 nm $MnFe_2O_4$ MNPs. $Fe(acac)_3$ (4 mmol, 1.4 g), Mn(acac)2 (2 mmol, 0.5 g), 1,2-hexadecanediol (10 mmol, 2.9 g), oleic acid (6 mmol, 1.9 mL), oleylamine (6 mmol, 2.8 mL), and 1-octadecene (20 mL) were mixed by stirring under N_2 flow (1 h). The mixture was then heated and kept at 200 °C for 2 h. Subsequently, the temperature was ramped to 280 °C to initiate particle formation. After reflux, the mixture was cooled to room temperature, and 2-propanol (80 mL) was added. Particles were collected *via* centrifugation (1811*g*, 15 min) and then dispersed in hexane. To make 12 nm particles *via* the seed-mediated growth, 10 nm $MnFe_2O_4$ MNPs (100 mg) were dispersed in hexane (10 mL) along with the same amount of metal acetylacetonates, 1,2-hexadecanediol, oleic acid, oleylamine, and 1-octadecene as described above. The mixture was heated and kept at 100 °C for 1 h under N_2 flow. The mixture was then heated and kept at 200 °C for 2 h. Finally, the temperature was increased to 300 °C, and the mixture was refluxed for 2 h. After cooling to room temperature, the particles were collected by the same washing and isolation procedure. $MnFe_2O_4$ MNPs of 16 nm were synthesized in a similar manner using 12 nm particles as a seed.

Fe@$MnFe_2O_4$ were prepared through annealing of manganese and iron oleate complexes on Fe nanoparticles.[19] Fe-only MNPs was first synthesized. A 20 mL amount of ODE and 0.3 mL of oleylamine (0.64 mmol) were mixed, and the mixture was heated (60 °C) under vacuum (1 h) and recharged with N_2 gas. The mixture was then heated to 260 °C. When the temperature became stable, $Fe(CO)_5$ (1.4 mL, 10 mmol) was injected. The solution was kept at 260 °C and under N_2 flow for 1 h, after which it was cooled to room temperature. While the Fe MNPs were formed, a manganese and iron oleate complex was separately prepared. $Mn_2(CO)_{10}$ (156 mg, 0.8 mmol), oleylamine (2.3 mL, 7.26 mmol), and 10 mL of ODE were mixed, and the mixture was heated to 60 °C under vacuum (1 h) and recharged with N_2. The mixture was heated to 120 °C, and $Fe(CO)_5$ (0.21 mL, 1.61 mmol) was subsequently injected. The solution, containing metal oleate complexes, was cooled to room temperature and transferred to the Fe MNP solution using double-ended needles. The mixture of Fe MNPs and metal oleate complexes was stirred (0.5 h) at room temperature. The reactor temperature was then ramped (5 °C/min) to the optimal annealing temperature (300 °C) for ferrite-shell formation. When the temperature stabilized, the mixture was stirred for 1 h. The solution was then cooled to room temperature, and 150 mL of 2-propanol solution (ODE/2-propanol = 0.2 v/v) was added. MNPs were collected *via* centrifugation (1811*g*, 15 min) and dispersed in 10 mL of hexane.

The shape, structure, and composition were further characterized using a transmission electron microscope (JEOL 2100, JEOL USA), an X-ray powder diffractometer (RU300, Rigaku), and an inductively coupled plasma atomic emission spectrometer (ICP-AES; Activa-S, HORIBA Jobin Yvon), respectively. The magnetic properties were analyzed using a vibrating sample magnetometer (EV-5, ADE Magnetics). The r_2 relaxivity of MNPs was obtained by measuring the R_2 of samples with varying MNP concentrations using a commercial relaxometer (0.47 T; Minispec mq20, Bruker). After the magnetic measurements, samples were dissolved in acid (HCl 10%), and the amounts of metals (Fe, Mn) were quantified by ICP-AES.

Surface Modification and Biotinylation. Amine-terminated CLIO nanoparticles were biotinylated in the presence of a 20-fold molar excess of sulfo-NHS-biotin (Pierce Biotechnology) in PBS containing 0.1 M sodium bicarbonate for 3 h at room temperature. Following conjugation, unbound biotin molecules were removed using Sephadex G50 columns (GE Healthcare).

All other MNPs prepared in the organic phase were transferred into the aqueous phase prior to biotinylation. Briefly, the prepared MNPs were suspended in 10 mL of chloroform and treated with 50 μL of triethylamine and dimercaptosuccinic acid (DMSA; 50 mg in 10 mL of DMSO). The mixture was incubated for 6 h at 40 °C until it gradually turned heterogeneous and precipitated down by centrifugation (3000 rpm, 10 min). The precipitate was washed with ethanol to remove excess DMSA and dispersed in 10 mL of ethanol. DMSA treatment was then repeated to improve nanoparticle aqueous stability. The precipitated MNPs were finally dispersed in 10 mL of water and had terminal sulfhydryl and carboxylic acid groups. The number of sulfhydryl groups per nanoparticle was ~50, as determined by Ellman's reagent (Pierce Biotechnology). To conjugate DMSA-treated MNPs with (+)biotin hydrazide (Aldrich), amide bonds

were formed using carboxylic acids in MNPs and amine groups in biotin through NHS/EDC chemical reactions. The DMSA-treated MNPs (25 mg) were dispersed in 10 mL of water, followed by the addition of NHS (3.5 mg), EDC (5 mg), and biotin (1 mg). The mixture was shaken for 3 h at room temperature. The conjugated MNPs was precipitated down (1811*g*, 20 min) and washed three times with water. The number of biotins per particle, quantified using the EZ Biotin Quantitation Kit (Pierce Biotechnology), was ~40.

MRSw Assays. Avidin (ImmunoPure Avidin #21121; Pierce Biotechnology) was first dissolved in PBS and serially diluted. MRSw samples were prepared by adding 100 μL of avidin solution, containing varying avidin doses, into biotinylated MNP solutions (100 μL). After 15 min of incubation at 37 °C, T_2 values of all samples were measured from 1 μL aliquots using a miniaturized nuclear magnetic resonance (NMR) system. Independently, the size of MNP clusters was measured *via* dynamic light scattering (Zetasizer Nano-ZS, Malvern). These experiments were then repeated using samples with different MNP concentrations. For the relaxation measurements, we used Carr−Purcell−Meiboom−Gill pulse sequences with the following parameters: echo time, 4 ms; repetition time, 6 s; number of 180° pulses per scan, 500; number of scans, 8.

Conflict of Interest: The authors declare no competing financial interest.

Acknowledgment. The authors thank N. Sergeyev for providing cross-linked dextran-coated iron oxide nanoparticles. H. S. acknowledges financial support from the B.S.-Ph.D. National Science Scholarship awarded by the Agency for Science, Technology and Research, Singapore. This work was supported in part by NIH grants (2R01EB004626, U01-HL080731, U54-CA119349, and T32-CA79443).

Supporting Information Available: Additional data from MRSw assays using DNA molecules and mathematical models describing MRSw assays for different types of MNPs. This material is available free of charge *via* the Internet at http://pubs.acs.org.

REFERENCES AND NOTES

1. Liotta, L. A.; Ferrari, M.; Petricoin, E. Clinical Proteomics: Written in Blood. *Nature* **2003**, *425*, 905.
2. Kingsmore, S. F. Multiplexed Protein Measurement: Technologies and Applications of Protein and Antibody Arrays. *Nat. Rev. Drug Discovery* **2006**, *5*, 310–320.
3. Fan, R.; Vermesh, O.; Srivastava, A.; Yen, B. K.; Qin, L.; Ahmad, H.; Kwong, G. A.; Liu, C. C.; Gould, J.; Hood, L.; Heath, J. R. Integrated Barcode Chips for Rapid, Multiplexed Analysis of Proteins in Microliter Quantities of Blood. *Nat. Biotechnol.* **2008**, *26*, 1373–1378.
4. Whitesides, G. M. The `Right' Size in Nanobiotechnology. *Nat. Biotechnol.* **2003**, *21*, 1161–1165.
5. Frey, N. A.; Peng, S.; Cheng, K.; Sun, S. Magnetic Nanoparticles: Synthesis, Functionalization, and Applications in Bioimaging and Magnetic Energy Storage. *Chem. Soc. Rev.* **2009**, *38*, 2532–2542.
6. Cheon, J.; Lee, J. H. Synergistically Integrated Nanoparticles as Multimodal Probes for Nanobiotechnology. *Acc. Chem. Res.* **2008**, *41*, 1630–1640.
7. Lee, H.; Sun, E.; Ham, D.; Weissleder, R. Chip-Nmr Biosensor for Detection and Molecular Analysis of Cells. *Nat. Med.* **2008**, *14*, 869–874.
8. Perez, J. M.; Josephson, L.; O'Loughlin, T.; Hogemann, D.; Weissleder, R. Magnetic Relaxation Switches Capable of Sensing Molecular Interactions. *Nat. Biotechnol.* **2002** *20*, 816–820.
9. Perez, J. M.; Josephson, L.; O'Loughlin, T.; Hogemann, D.; Weissleder, R. Magnetic Relaxation Switches Capable of Sensing Molecular Interactions. *Nat. Biotechnol.* **2002** *20*, 816–820.
10. Sun, E. Y.; Weissleder, R.; Josephson, L. Continuous Analyte Sensing with Magnetic Nanoswitches. *Small* **2006**, *2*, 1144–1147.
11. Colombo, M.; Ronchi, S.; Monti, D.; Corsi, F.; Trabucchi, E.; Prosperi, D. Femtomolar Detection of Autoantibodies by Magnetic Relaxation Nanosensors. *Anal. Biochem.* **2009**, *392*, 96–102.
12. Atanasijevic, T.; Shusteff, M.; Fam, P.; Jasanoff, A. Calcium-Sensitive MRI Contrast Agents Based on Superparamagnetic Iron Oxide Nanoparticles and Calmodulin. *Proc. Natl. Acad. Sci. U. S. A.* **2006**, *103*, 14707–14712.
13. Taktak, S.; Sosnovik, D.; Cima, M. J.; Weissleder, R.; Josephson, L. Multiparameter Magnetic Relaxation Switch Assays. *Anal. Chem.* **2007**, *79*, 8863–8869.
14. Kaittanis, C.; Santra, S.; Santiesteban, O. J.; Henderson, T. J.; Perez, J. M. The Assembly State Between Magnetic Nanosensors and Their Targets Orchestrates Their Magnetic Relaxation Response. *J. Am. Chem. Soc.* **2011**, *133*, 3668–3676.
15. Shapiro, M. G.; Atanasijevic, T.; Faas, H.; Westmeyer, G. G.; Jasanoff, A. Dynamic Imaging With Mri Contrast Agents: Quantitative Considerations. *Magn. Reson. Imaging* **2006**, *24*, 449–462.
16. Josephson, L.; Tung, C. H.; Moore, A.; Weissleder, R. High-Efficiency Intracellular Magnetic Labeling with Novel Superparamagnetic-Tat Peptide Conjugates. *Bioconjugate Chem.* **1999**, *10*, 186–191.
17. Sun, S.; Zeng, H.; Robinson, D. B.; Raoux, S.; Rice, P. M.; Wang, S. X.; Li, G. Monodisperse MFe_2O_4 (M = Fe, Co, Mn) Nanoparticles. *J. Am. Chem. Soc.* **2004**, *126*, 273–279.
18. Lee, H.; Yoon, T. J.; Figueiredo, J. L.; Swirski, F. K.; Weissleder, R. Rapid Detection and Profiling of Cancer Cells in Fine-Needle Aspirates. *Proc. Natl. Acad. Sci. U. S. A.* **2009**, *106*, 12459–12464.
19. Yoon, T. J.; Lee, H.; Shao, H.; Weissleder, R. Highly Magnetic Core-Shell Nanoparticles With a Unique Magnetization Mechanism. *Angew. Chem., Int. Ed.* **2011**, *50*, 4663–4666.
20. Gillis, P.; Moiny, F.; Brooks, R. A. On T(2)-Shortening By Strongly Magnetized Spheres: A Partial Refocusing Model. *Magn. Reson. Med.* **2002**, *47*, 257–263.
21. Issadore, D.; Min, C.; Liong, M.; Chung, J.; Weissleder, R.; Lee, H. Miniature Magnetic Resonance System for Point-of-Care Diagnostics. *Lab Chip* **2011**, *11*, 2282–2287.
22. Brooks, R. A. T(2)-Shortening By Strongly Magnetized Spheres: A Chemical Exchange Model. *Magn. Reson. Med.* **2002**, *47*, 388–391.
23. Kim, G. Y.; Josephson, L.; Langer, R.; Cima, M. J. Magnetic Relaxation Switch Detection of Human Chorionic Gonadotrophin. *Bioconjugate Chem.* **2007**, *18*, 2024–2028.
24. Yablonskiy, D. A.; Haacke, E. M. Theory of NMR Signal Behavior in Magnetically Inhomogeneous Tissues: The Static Dephasing Regime. *Magn. Reson. Med.* **1994**, *32*, 749–763.
25. Witten, T. A.; Sander, L. M. Diffusion-Limited Aggregation, a Kinetic Critical Phenomenon. *Phys. Rev. Lett.* **1981**, *47*, 1400–1403.
26. Halsey, T. C. Diffusion-Limited Aggregation: A Model for Pattern Formation. *Phys. Today* **2000**, *53*, 36.
27. Schaefer, D. W.; Martin, J. E.; Wiltzius, P.; Cannell, D. S. Fractal Geometry of Colloidal Aggregates. *Phys. Rev. Lett.* **1984**, *52*, 2371–2374.
28. Zhou, C.; Zhao, Y.; Jao, T.-C.; Winnik, M. A.; Wu, C. Photo-induced Aggregation of Polymer Nanoparticles in a Dilute Nonaqueous Dispersion. *J. Phys. Chem. B* **2002**, *106*, 1889–1897.
29. Gustav, v., S.; Benedek, G.; Ralph., D., B. Measurement of the Cluster Size Distributions for High Functionality Antigens Cross-Linked By Antibody. *Macromolecules* **1980**, *13*, 939–945.
30. Koh, I.; Hong, R.; Weissleder, R.; Josephson, L. Nanoparticle-Target Interactions Parallel Antibody-Protein Interactions. *Anal. Chem.* **2009**, *81*, 3618–3622.
31. Dodds, P.; Weitz, J. Packing-Limited Growth. *Phys. Rev. E* **2002**, *65*,
32. Nam, J. M.; Thaxton, C. S.; Mirkin, C. A. Nanoparticle-Based Bio-Bar Codes for the Ultrasensitive Detection of Proteins. *Science* **2003**, *301*, 1884–1886.

33. Koh, I.; Hong, R.; Weissleder, R.; Josephson, L. Sensitive Nmr Sensors Detect Antibodies to Influenza. *Angew. Chem., Int. Ed.* **2008**, *47*, 4119–4121.
34. Kulkarni, A. A.; Weiss, A. A.; Iyer, S. S. Detection of Carbohydrate Binding Proteins Using Magnetic Relaxation Switches. *Anal. Chem.* **2010**, *82*, 7430–7435.
35. Josephson, L.; Tung, C.-H.; Moore, A.; Weissleder, R. High-Efficiency Intracellular Magnetic Labeling with Novel Superparamagnetic-Tat Peptide Conjugates. *Bioconjugate Chem.* **1999**, *10*, 186–191.